



UvA-DARE (Digital Academic Repository)

Optical phonons and magnetoelastic coupling in the ionic conductor AgCrSe₂

Groefsema, J.; Feng, X.; Morice, C.; Huang, Y.; van Heumen, E.

DOI

[10.1103/PhysRevMaterials.6.115402](https://doi.org/10.1103/PhysRevMaterials.6.115402)

Publication date

2022

Document Version

Final published version

Published in

Physical Review Materials

[Link to publication](#)

Citation for published version (APA):

Groefsema, J., Feng, X., Morice, C., Huang, Y., & van Heumen, E. (2022). Optical phonons and magnetoelastic coupling in the ionic conductor AgCrSe₂. *Physical Review Materials*, 6(11), [115402]. <https://doi.org/10.1103/PhysRevMaterials.6.115402>

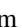


General rights

It is not permitted to download or to forward/distribute the text or part of it without the consent of the author(s) and/or copyright holder(s), other than for strictly personal, individual use, unless the work is under an open content license (like Creative Commons).

Disclaimer/Complaints regulations


If you believe that digital publication of certain material infringes any of your rights or (privacy) interests, please let the Library know, stating your reasons. In case of a legitimate complaint, the Library will make the material inaccessible and/or remove it from the website. Please Ask the Library: <https://uba.uva.nl/en/contact>, or a letter to: Library of the University of Amsterdam, Secretariat, Singel 425, 1012 WP Amsterdam, The Netherlands. You will be contacted as soon as possible.

Optical phonons and magnetoelastic coupling in the ionic conductor AgCrSe_2

Jim Groefsema ¹, Xuanbo Feng (馮翹博) ^{1,2}, Corentin Morice,¹ Yingkai Huang,¹ and Erik van Heumen ^{1,2,*}

¹*Institute of Physics, University of Amsterdam, Science Park 904, 1098 XH Amsterdam, The Netherlands*

²*QuSoft, Science Park 123, 1098 XG Amsterdam, The Netherlands*

 (Received 31 August 2022; revised 4 October 2022; accepted 5 October 2022; published 3 November 2022)

AgCrSe_2 is an example of a superionic conductor that has recently attracted attention for its low thermal conductivity. Here we investigate the optical properties of AgCrSe_2 in the ordered phase between 14 K and 374 K using reflectivity experiments and compare them to the optical conductivity obtained from electronic structure calculations. The far infrared optical response is dominated by three phonon modes, while six interband transitions are observed in the visible range. We find good agreement between the experimental interband transitions and the calculated optical transitions. From our analysis we find that the phonon parameters display an interesting temperature dependence around the Néel temperature, pointing to a small magnetoelastic coupling. In addition, the lifetimes of the modes indicate that three-phonon processes dominate and the optical phonons decay into low-energy acoustic modes involved in the superionic transition. Finally, we detect a small free charge carrier response through the analysis of Fabry-Perot interference fringes in our reflectivity data.

DOI: [10.1103/PhysRevMaterials.6.115402](https://doi.org/10.1103/PhysRevMaterials.6.115402)

I. INTRODUCTION

With an increasing demand for batteries, solid-state ionic conductors have gained in interest due to their higher energy density, a potential for fast charging, and increased safety over commonly used Li-ion batteries [1]. Current in solid-state ionic conductors is carried by mobile ions through hopping between vacant sites in the material, which is typically a slow process. This has led to the study of a small group of materials that partially “melt” above the so-called superionic transition. Above this transition, the energy landscape of a sublattice of ions in the structure changes such that ions can rapidly diffuse through correlated motion [2]. As it turns out, superionic conductors also have excellent thermoelectric response, owing to a very low thermal conductivity resulting from the partially molten sublattice of ions [3].

One example of such a superionic conductor with excellent thermoelectric figure of merit is AgCrSe_2 , which consists of a sublattice of Ag ions sandwiched between CrSe_2 layers [4]. At a temperature of 475 K, AgCrSe_2 transitions into its superionic phase, where Ag ions become disordered [5–7]. The phase transition into the disordered phase is second order [6], but diffusion of Ag ions already seems to start well below the transition [8]. The diffusion of Ag ions is promoted by lowering of the energy barrier for the occupation of a second interstitial site in the Ag lattice and has been proposed to result in the breakdown of certain phonon modes [9]. However, direct imaging of the occupation of interstitial sites by Ag ions with transmission electron microscopy suggests that slow diffusion is a result of disorder [10]. At low temperature, the Cr spins order in a noncollinear antiferromagnetic order with antiferromagnetic stacking along the c axis [5] and fluctuations

of this order persisting up to 200 K [11]. Recently, short range correlations and the interplay between spin-orbit coupling and magnetic order have been studied at low temperatures [12,13].

The low thermal conductivity is most likely determined by the phonon spectrum, and several momentum resolved studies have indeed observed changes in the phonon spectrum with temperature [8,9,11]. An early far-infrared optical study on sintered samples focused on the high-temperature transition and its impact on the phonon spectrum, reporting changes in the transverse optical-longitudinal optical (TO-LO) mode splitting [14]. More recently, indications of the important role played by a 3 meV phonon mode and a possible magnetoelastic coupling between the low-energy phonons and antiferromagnetic fluctuations have been brought to light [11]. This led us to revisit AgCrSe_2 using high-resolution optical spectroscopy reflectivity experiments on single crystalline samples, with a particular focus on the optical phonon modes and their temperature dependence. In this letter, we report reflectivity measurements between 14 K and 374 K, covering the low-temperature antiferromagnetic state, but not the high-temperature superionic transition. Three phonon modes are observed in the far infrared region and we find evidence for a weak magnetoelastic coupling through a detailed temperature dependence of the phonon mode parameters. We report the interband optical response and compare these to electronic structure calculations. Finally, we observe Fabry-Perot interference fringes in the reflectivity data. From a detailed analysis of these fringes, we are able to deduce a small free charge contribution to the optical response resulting in a dc resistivity of 0.5 Ω cm.

II. EXPERIMENTAL METHODS

Single crystal AgCrSe_2 samples were produced using the chemical vapor transport growth method. The resulting

*e.vanheumen@uva.nl

AgCrSe₂ samples have the approximate dimensions of 3 × 3 mm with an average thickness between 100 and 200 μm. The crystal is supported by a copper holder, which has the shape of a tapered cone with the flat top surface cut to the shape of the AgCrSe₂ sample. In this way, light reflected from the copper holder will not reach the detector. The holder was polished to a smooth finish and cleaned using ultrasonic cleaning with a series of solutions in the order of citric acid, acetone, and ethanol. Conducting silver epoxy was used to glue the sample to the holder and was subsequently baked at 125 °C for 20 minutes.

AgCrSe₂ does not cleave and is too soft to polish, therefore the as-grown surface was used for experiments. Fortunately, these surfaces naturally have a mirror smooth finish that is suitable for reflectivity measurements. The reflectivity data was obtained using a VERTEX 80v FTIR spectrometer over the photon energy range from 4 meV to 3 eV, using different light sources and detectors. The temperature dependence was measured using cooling and heating cycles between 14 K and 374 K at a rate of 1.66 K per minute. The heating and cooling stages have been repeated multiple times for the different photon energy ranges to improve the signal-to-noise ratio. In order to obtain a reference spectrum, gold or silver is evaporated on the sample surface. A new measurement using the same parameters and procedures as used for the sample measurement was then performed to obtain the reference spectrum. While it is possible to cleave aluminum and gold off the sample, cleaving silver turns out to be rather difficult. Due to this, more than two different samples from the same batch were used. The reflectivity obtained in this way agreed very well in the ranges of overlap between different samples.

Electronic structure calculations of AgCrSe₂ are reported using density functional theory and an all-electron full-potential linearized augmented plane-wave basis set as implemented in Elk [15]. We employed the generalized gradient approximation in the shape of the Perdew, Burke, and Ernzerhof functional [16], including spin-orbit coupling. We use a predefined high-quality set of parameters, and a Monkhorst-Pack grid of 16 × 16 × 16 **k** points in the Brillouin zone, which were checked for convergence. Calculations were done in the primitive unit cell, with ferromagnetic spin order, using an experimentally measured crystal structure [5]. Ferromagnetic ordering was chosen since the antiferromagnetic coupling cannot be observed in single-unit-cell calculations and the change between ferromagnetic and antiferromagnetic ground states is low enough to be neglected. We find a magnetic moment of 3μ_B [17]. Based on these results, we calculated the optical conductivity within the random phase approximation without local field effects, using a shifted grid of 20 × 20 × 20 **k** points and a smearing width of 50 meV.

III. RESULTS

Figure 1 shows the reflectivity against photon energy for a selection of temperatures. In the photon energy range above 0.5 eV, the reflectivity shows several broad, temperature-dependent structures that correspond to interband transitions. The inset of Fig. 1 shows the far-infrared (FIR) reflectivity data from 4 meV to 50 meV. Three structures are visible,

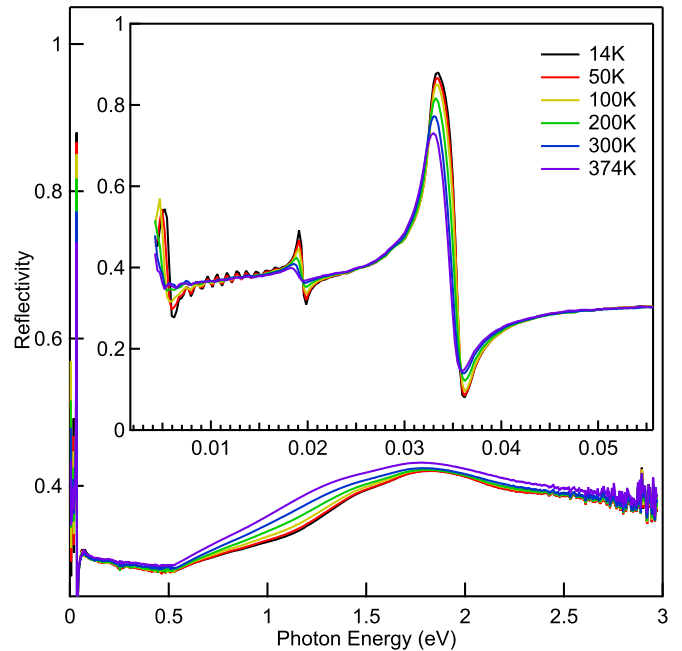


FIG. 1. The measured reflectivity against the photon energy used for selected temperatures. Interband transitions can be observed around 1 eV and 1.5 eV. The inset shows the reflectivity at a photon energy range of 4–50 meV. Three phonons are observed with smaller oscillations between 5 meV and 15 meV.

corresponding to the three infrared active optical phonons expected for AgCrSe₂ [18,19]. Each of the modes shows significant temperature dependence, broadening as the temperature is increased. As we will show in more detail below, these phonon modes can be well described by symmetric Lorentz modes, hinting at a weak electron-phonon coupling. The phonon modes appear to be unscreened by an electronic background (corresponding to free charge density) and the reflectivity spectrum resembles that of an insulator. This is further supported by a series of small oscillations that can be observed most clearly between 5 meV and 15 meV at low temperature. As we will show below, these correspond to Fabry-Perot interference fringes and are a further indicator that has very small free charge density. As the temperature increases these fringes become weaker, but they remain visible up to the highest measured temperature.

The first step in our analysis consists of creating a series of Drude-Lorentz models, one for each temperature, with parameters optimized using a least-squares optimization routine [20]. An accurate description of the reflectivity is obtained with a Drude-Lorentz model consisting of a total of nine Lorentz oscillators, describing three phonon modes and six interband transitions. The first interband transition appears in the mid infrared around 0.2–0.3 eV, while the other transitions are closer to the visible light range with an onset around 0.7 eV. The Drude-Lorentz model parameters for 14 K, 100 K, 300 K, and 374 K are presented in Table I. The Drude-Lorentz model provides the basis for the second step in our analysis. We used a variational dielectric function to effectively perform the Kramers-Kronig transformation and calculate the

TABLE I. Parameters for the optimized Drude-Lorentz model at selected temperatures. All parameters are in meV. ϵ_∞ is set to 2.83 for all temperatures. The Drude term makes use of the parameters ω_p and γ_D , corresponding to the plasma frequency and scattering rate, respectively. The other parameters presented are the eigenfrequency Ω_0 , scattering rate γ , and oscillator strength f . (*) The parameters of the Drude term are obtained from the analysis of the Fabry-Perot fringes of the 14 K data and have not been optimized at other temperatures.

Temperature		14 K	100 K	300 K	374 K
Drude*	ω_p	12.03	12.03	12.03	12.03
	γ_D	12.40	12.40	12.40	12.40
Phonon 1	Ω_0	5.28	4.74	4.59	4.60
	f	9.28	9.35	7.10	5.28
	γ	0.58	0.71	1.33	1.13
Phonon 2	Ω_0	19.24	19.23	18.98	18.88
	f	13.58	13.09	13.08	11.15
	γ	0.55	0.86	2.01	2.09
Phonon 3	Ω_0	32.72	32.71	32.39	32.25
	f	51.95	51.85	51.01	50.80
	γ	0.44	0.61	0.98	1.17
Lorentz 1	Ω_0	306	280	224	199
	f	574	518	394	320
	γ	879	850	643	459
Lorentz 2	Ω_0	866	1284	1328	1335
	f	178	625	1054	1167
	γ	128	340	281	264
Lorentz 3	Ω_0	1032	1022	1132	1152
	f	392	403	617	754
	γ	245	250	243	233
Lorentz 4	Ω_0	1480	1487	1514	15245
	f	1452	1412	1341	1422
	γ	475	425	356	349
Lorentz 5	Ω_0	1771	1771	1771	1771
	f	3422	3418	3370	3365
	γ	745	745	745	745
Lorentz 6	Ω_0	2413	2413	2413	2413
	f	4066	4066	4066	4066
	γ	1432	1432	1432	1432

optical conductivity $\hat{\sigma}(\omega, T)$ [20]. Figure 2 shows $\sigma_1(\omega, T)$ plotted against photon energy on a log-log scale from 3 meV up to 1 eV. The far infrared is characterized by three phonon modes on top of a small, but finite, background conductivity of a few $\Omega^{-1} \text{cm}^{-1}$. The conductivity steadily starts to increase above 10 meV, possibly with some small structure around 0.1 eV. Above 0.5 eV, the conductivity starts to increase more rapidly. This energy gap is in good agreement with estimates based on static measurements [6]. The inset shows $\sigma_1(\omega, T)$ on a linear photon energy scale up to 3 eV.

Figure 3 a shows the unit cell and corresponding first Brillouin zone in which the high symmetry points are labeled. Figure 3 shows the electronic structure, calculated along several high symmetry lines of the Brillouin zone. The calculations point to a small indirect band gap of about 0.17 eV. To compare the electronic structure calculations with our experiments, we compute the optical conductivity within the random phase approximation. The result is summarized in Fig. 4. Figure 4(a) shows the measured optical conductivity

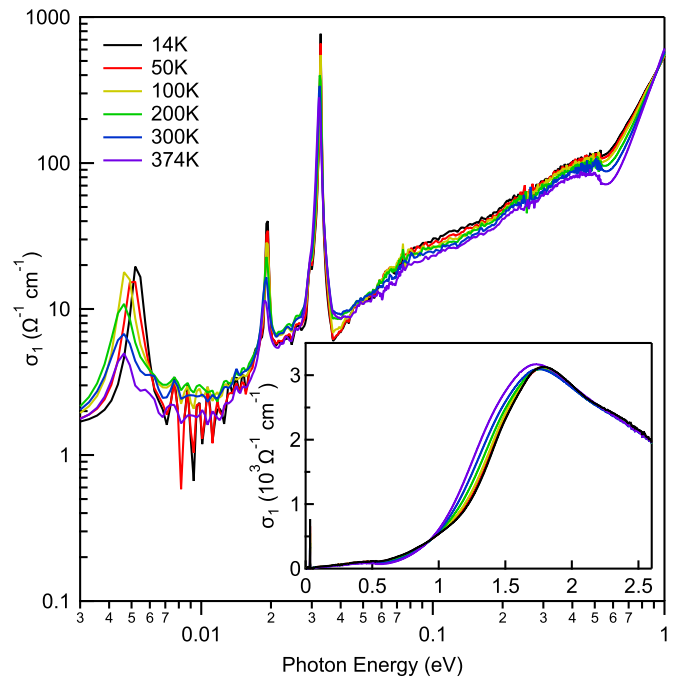


FIG. 2. The real part of the optical conductivity $\sigma_1(\omega, T)$, plotted against photon energy on a log-log scale. We observe three phonon modes in the infrared (see Table I), and at low temperature a number of Fabry-Perot interference fringes (see main text for details). The inset shows the optical conductivity over the full energy range.

together with the Drude-Lorentz model fit. Also shown is the decomposition of the fit in individual oscillators that contribute to the conductivity. We use the resonance frequencies of these oscillators to compare to the calculated optical conductivity as presented in Fig. 4(b). The calculated conductivity has a slightly different overall shape, but qualitatively it seems to be in good agreement with the measured optical response. The energies of the experimentally obtained interband transitions (dashed vertical lines) closely correspond to transitions in the calculations. In particular, the lowest interband transition that is observed experimentally closely agrees with the onset of interband transitions in the calculation [see inset of Fig. 4(b)]. This agreement suggests that the size of the indirect band gap obtained from the calculations is likely close to the actual value.

IV. DISCUSSION

As mentioned in the introduction, the ionic conductivity in AgCrSe_2 is driven by delocalization of the Ag ions, which are sandwiched between CrSe_2 layers. At low temperatures the Ag ions form a regular triangular lattice, while at high temperatures a second triangular lattice becomes partially occupied, forming a honeycomb lattice. There are six infrared active phonons associated with this structure, of which three are in-plane modes [18]. The phonon dispersions and partial phonon density of states have been previously calculated in Refs. [8,21]. These predict that IR active phonon modes may be expected around 5 meV, 17 meV, and 30 meV [21]. The projected phonon density of states suggests that the lowest of these modes involves the motion of Ag ions, while the higher-energy modes are mainly of Se character [8].

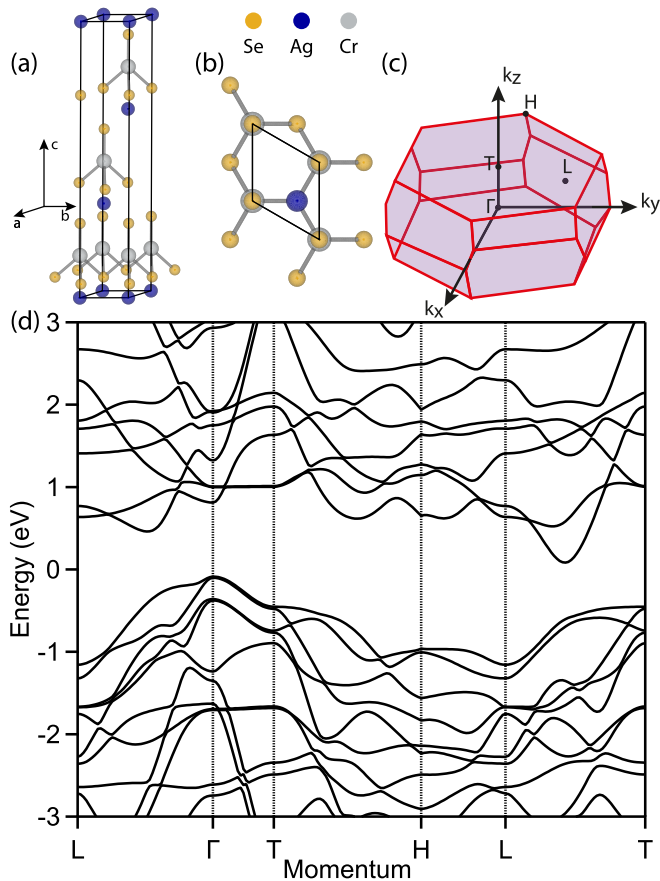


FIG. 3. (a–c) from left to right, (a) crystal structure viewed along the b axis (Ag in blue, Cr in gray, and Se in orange), (b) crystal structure viewed along the c axis, and (c) the Brillouin zone with several high symmetry points indicated. (d) The electronic band structure of AgCrSe_2 calculated along high symmetry lines. An indirect band gap of 0.17 eV is observed, with the valence band maximum at Γ and the conduction band minimum along the L - T line.

Our Drude-Lorentz model provides direct access to the temperature-dependent phonon parameters and they are displayed in Fig. 5. The three phonon modes observed have eigenfrequencies of 5.2 (phonon 1), 19.2 (phonon 2), and 32.7 meV (phonon 3) at the lowest temperature, in good agreement with the calculations. The observation of the 19.2 meV mode corresponds well with the TO mode observed in Ref. [8]. In Figs. 5(a)–5(c) the temperature dependence of these modes is shown. As the temperature increases, the modes soften, as may be expected from increased thermal motion of the ions involved.

The temperature-dependent oscillator strengths of these modes are shown in Figs. 5(d)–5(e). At high temperatures the modes decrease in strength approximately as $f(T) = A - T^2$, which is typical for phonon modes. Interestingly, the phonon modes 2 and 3 show a small but marked increase in strength below approximately 60 K (indicated by red guide to the eye). This coincides with the temperature where the eigenfrequency reaches a maximum and is close to the Néel temperature at 55 K. Given that these modes have significant Se character and some Cr character, this could point to a small magnetoelastic coupling that was inferred from the correlation of negative thermal expansion with the onset of anti-ferromagnetic order

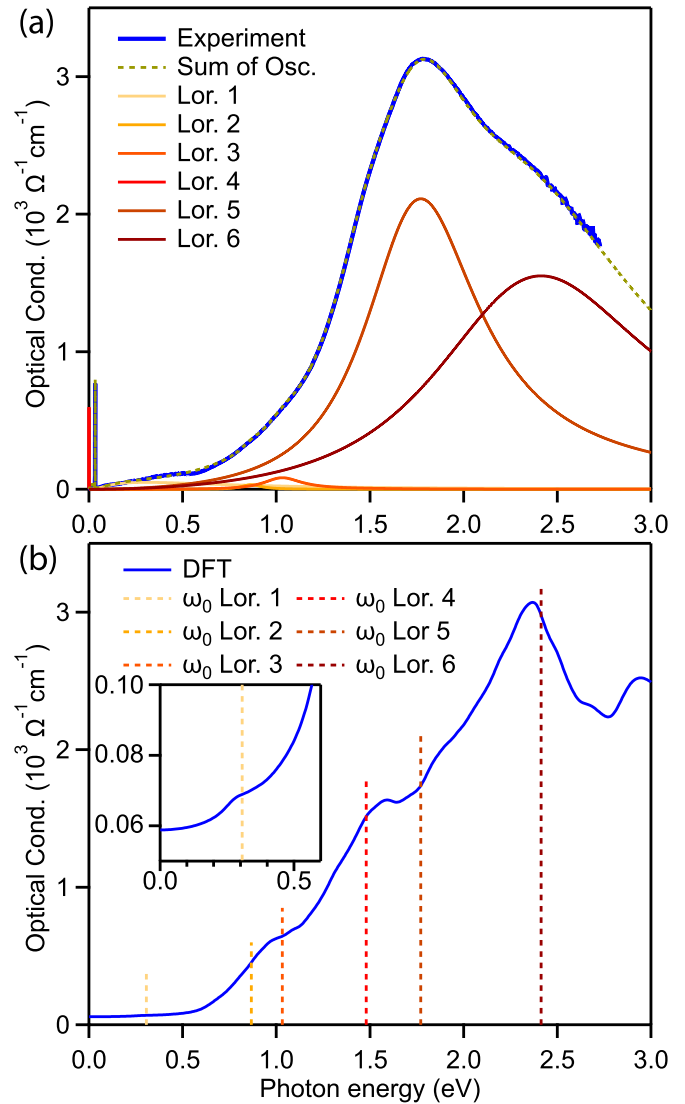


FIG. 4. (a) Experimental optical conductivity at 14 K and decomposition in interband transitions. Also shown is the sum of the individual oscillators (dashed yellow line) compared to the experimental data (blue line). (b) Comparison of the optical response calculated in the random phase approximation with experimental oscillator positions. Dashed lines indicate approximate interband transitions determined from the oscillators in (a). The inset shows that the transition associated with the indirect band gap in the calculation around 0.2 eV corresponds well with the onset of interband transitions in the experimental data.

[11]. The absence of an enhancement for phonon mode 1, which is of mostly Ag character, further supports the interaction of spin and lattice. Next, we turn to the phonon line widths, which at the lowest temperature are all close to being resolution limited and approximately 4 cm^{-1} (or 8.3 ps). As temperature increases, these line widths increase and reach values at 374 K of 8 cm^{-1} (4.2 ps), except for the 19.2 meV mode that broadens to 16 cm^{-1} (2.1 ps). Previous works have focused on the lifetime associated with the (acoustic) phonon modes in order to determine the origin of the low thermal conductivity [8,10,21]. From our detailed temperature-dependent measurements, we can extract the lifetime of the IR active

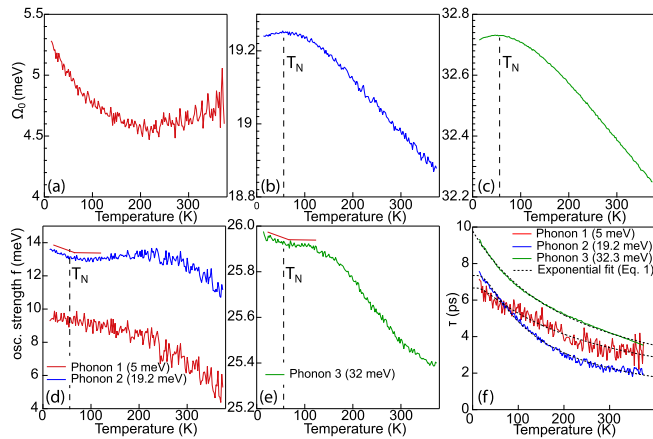


FIG. 5. Eigenfrequency Ω_0 for phonon mode 1 (a), phonon 2 (b), and phonon 3 (c). Panels (d) and (e) display the corresponding oscillator strengths f . The vertical dashed lines in panels (a)–(e) indicate the Néel temperature. The red lines in panels (d) and (e) are a guide to the eye for the change of slope in the temperature dependence of the oscillator strength. Panel (f) shows the lifetimes associated with the phonon modes as a function of temperature together with fits to Eq. 1 (dashed black lines).

modes. In the simplest case, three-phonon scattering dominates and we therefore make use of the temperature-dependent line width proposed in Refs. [22,23],

$$\Gamma(T) = \Gamma_0 + A \left(1 + \frac{2}{e^{(\Omega_0 - \Omega_1)/k_B T} - 1} + \frac{2}{e^{\Omega_1/k_B T} - 1} \right) \quad (1)$$

where Γ_0 and A are the intrinsic line width due to disorder and an anharmonic constant. This describes the line width broadening of an optical phonon with initial energy Ω_0 into two phonon modes. One of these modes has a final energy Ω_1 , and energy conservation thus demands that the second mode has energy $\Omega_0 - \Omega_1$.

We use Eq. [1] to fit the temperature-dependent lifetimes of the three phonon modes in Fig. 5. Since the intrinsic phonon energy can be derived from the Drude-Lorentz model parameters (Ω_0 in Table I), we can extract Ω_1 from our data. We then obtain the phonon energy scales $\Omega_1 \approx 3.0$ meV, 12.7 meV, and 32.5 meV for phonons 1, 2, and 3 respectively. The differences are approximately $\Omega_0 - \Omega_1 \approx 2$ meV, 6.5 meV, and 0.1 meV. Given that these energies are well below the optical branches, the above analysis indicates that the optical phonons decay into the low-energy acoustic modes that are believed to be involved in the superionic transition [8]. The comparison with the data is somewhat better at high temperatures, where the decrease in the lifetime slows down significantly faster than expected from four-phonon scattering processes.

To conclude our discussion, we briefly return to the small oscillations observed in the reflectivity data. Our initial analysis assumes that our crystal is optically infinitely thick. However, the free charge density is very small and according to previous work and our own band structure calculations,

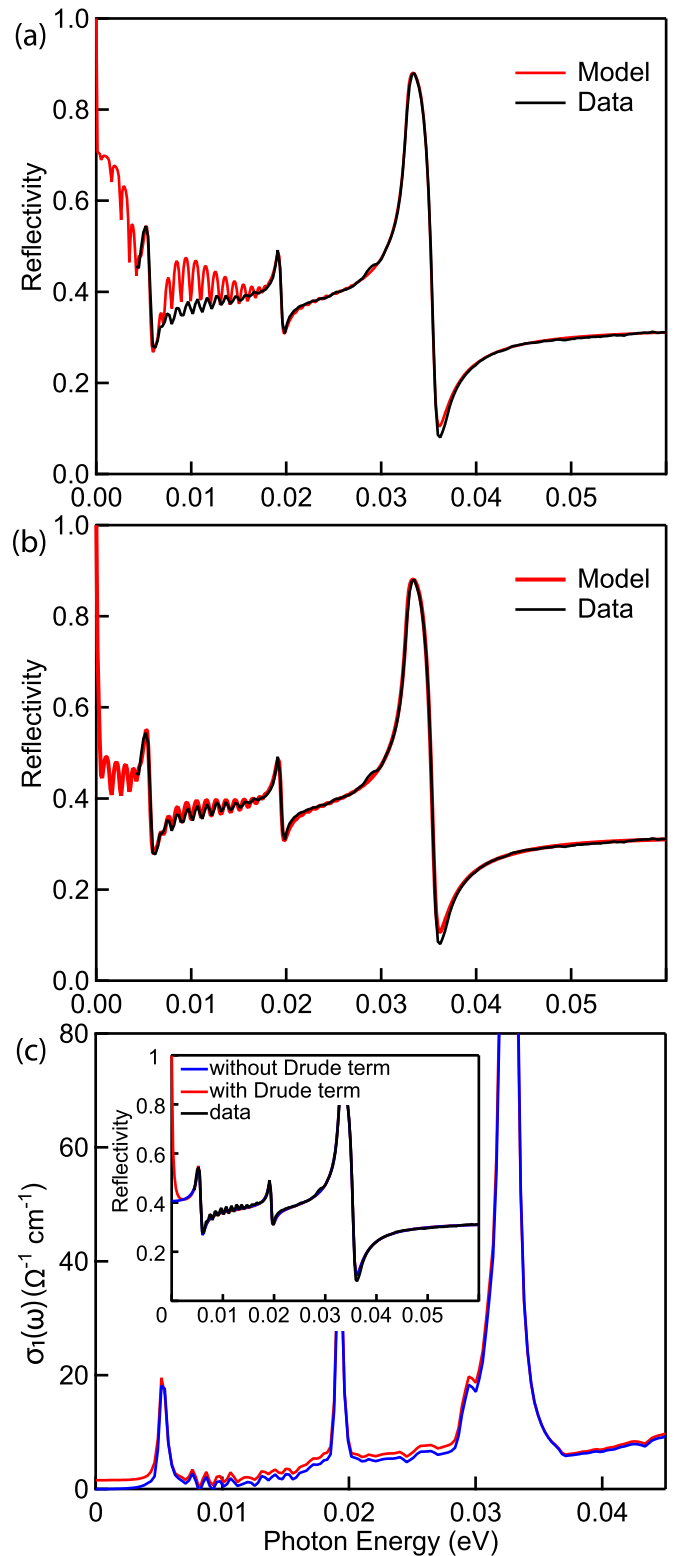


FIG. 6. (a) Model calculation of Fabry-Perot interference pattern compared to experimental data based on the Drude-Lorentz model obtained from initial fits. (b) The same calculation, but now with an additional Drude response added to the model. (c) Optical conductivity with and without Drude response. The inset shows the difference between the two models imprinted on the reflectivity.

AgCrSe₂ should be insulating. If the screening is small and the sample thin, light can propagate through the sample and reflect off the copper sample holder supporting the sample. This reflected light can interfere with the light reflecting off the sample surface at the first reflection, giving rise to Fabry-Perot interference fringes. These fringes contain additional information on the optical properties of the sample as their amplitude and period are determined by the dielectric function. For this purpose, we use the original Drude-Lorentz model presented in Table I as input for the dielectric model of the AgCrSe₂ sample. For the Cu holder, we assume that it is infinitely thick and has a simple Drude response with typical parameters for a good metal: $\omega_p=4$ eV and $\Gamma=0.07$ eV. These two models are used as input for a multilayer dielectric function model from which we obtain the reflectivity.

Figure 6(a) shows the comparison between the multilayer model and the measured reflectivity at 14 K. To get the period of the model to agree with the data we used a sample thickness of 130 μm , which is consistent with measurements of the sample. Although the period of the oscillations matches well with the data, there is a significant discrepancy in the overall shape of the reflectivity. This is due to higher-order reflections contributing and resulting in a beating pattern. We found that the only way to suppress these beatings was to introduce a small Drude response to the Drude-Lorentz model of the AgCrSe₂ crystal. The corresponding model is shown in Fig. 6(c), while the parameters of the Drude term are listed in Table I. This small Drude response introduces a finite dc conductivity of approximately $2 \Omega^{-1}\text{cm}^{-1}$, which is smaller than found in previous studies [4]. The finite conductivity is likely linked to Ag vacancies, resulting in a depletion of the valence band. The low conductivity therefore points to only a small Ag vacancy and the good quality of our crystal. The plasma frequency obtained from our fit corresponds to a carrier density $n_{\text{eff}} \approx 1.1 \times 10^{17} \text{ cm}^{-3}$, placing it well below the

regime where a large positive magnetoresistance was observed [13]. Finally, we note that the presence of the Drude response could not have been detected based on our reflectivity data alone. As the inset of Fig. 6(c) shows, the original Drude-Lorentz model and the model with Drude response give the same level of agreement with our experimental data.

V. SUMMARY

To summarize our findings, we have measured the reflectivity for AgCrSe₂ over the photon energy range of 4 meV to 3 eV between 14 K and 375 K. Three phonon modes are observed with eigenfrequencies of 5.2 meV, 19.2 meV, and 32.7 meV at low temperature. These modes soften slightly as the temperature increases. The oscillator strength shows a small increase with decreasing temperature close to the Néel temperature, possibly indicating a weak magnetoelastic coupling. The temperature dependence of the line width suggests that four-phonon scattering is less important than three-phonon scattering in the temperature range of our experiments. Assuming that three-phonon processes dominate, the temperature dependence is compatible with coupling to low-energy acoustic modes. The optical gap is approximately 0.5 eV and we have reported three interband transition in the visible light part of the spectrum. Finally, we observe Fabry-Perot interference fringes in the reflectivity data that enable us to determine a free carrier density that provides a small contribution to the dc conductivity.

ACKNOWLEDGMENTS

The authors thank the Institute of Physics and H. Ellermeijer for continued support. This work is supported by the research center for quantum software QuSoft.

-
- [1] S. Ohno, A. Banik, G. F. Dewald, M. A. Kraft, T. Krauskopf, N. Minafra, P. Till, M. Weiss, and W. G. Zeier, *Prog. Energy* **2**, 022001 (2020).
 - [2] X. He, Y. Zhu, and Y. Mo, *Nat. Commun.* **8**, 15893 (2017).
 - [3] T. P. Bailey and C. Uher, *Curr. Opin. Green Sustain. Chem.* **4**, 58 (2017).
 - [4] F. Gascoin and A. Maignan, *Chem. Mater.* **23**, 2510 (2011).
 - [5] F. M. R. Engelsman, G. A. Wiegers, F. Jellinek, and B. Van Laar, *J. Solid State Chem.* **6**, 574 (1973).
 - [6] B. Boukamp and G. Wiegers, *Solid State Ionics* **9-10**, 1193 (1983).
 - [7] A. Van Der Lee and G. A. Wiegers, *J. Solid State Chem.* **82**, 216 (1989).
 - [8] B. Li, H. Wang, Y. Kawakita, Q. Zhang, M. Feygenson, H. L. Yu, D. Wu, K. Ohara, T. Kikuchi, K. Shibata *et al.*, *Nat. Mater.* **17**, 226 (2018).
 - [9] J. Ding, J. L. Niedziela, D. Bansal, J. Wang, X. He, A. F. May, G. Ehlers, D. L. Abernathy, A. Said, A. Alatas *et al.*, *Proc. Natl. Acad. Sci.* **117**, 3930 (2020).
 - [10] L. Xie, D. Wu, H. Yang, Y. Yu, Y. Wang, and J. He, *J. Mater. Chem. C* **7**, 9263 (2019).
 - [11] F. Damay, S. Petit, S. Rols, M. Braendlein, R. Daou, E. Elkaim, F. Fauth, F. Gascoin, C. Martin, and A. Maignan, *Sci. Rep.* **6**, 23415 (2016).
 - [12] M. Baenitz, M. M. Piva, S. Luther, J. Sichelschmidt, K. M. Ranjith, H. Dawczak-Debicki, M. O. Ajeesh, S.-J. Kim, G. Siemann, C. Bigi *et al.*, *Phys. Rev. B* **104**, 134410 (2021).
 - [13] H. Takahashi, T. Akiba, A. H. Mayo, K. Akiba, A. Miyake, M. Tokunaga, H. Mori, R. Arita, and S. Ishiwata, *Phys. Rev. Mater.* **6**, 054602 (2022).
 - [14] K. Wakamura, K. Hirokawa, and K. Orita, *J. Phys. Chem. Solids* **57**, 75 (1996).
 - [15] The Elk Code, <http://elk.sourceforge.net/>.
 - [16] J. P. Perdew, K. Burke, and M. Ernzerhof, *Phys. Rev. Lett.* **77**, 3865 (1996).
 - [17] U. K. Gautam, R. Seshadri, S. Vasudevan, and A. Maignan, *Solid State Commun.* **122**, 607 (2002).

- [18] K. Wakamura, K. Hirokawa, H. Shima, and K. Takarabe, *Solid State Ionics* **40-41**, 331 (1990).
- [19] C. Wang and Y. Chen, *Npj Comput. Mater.* **6**, 26 (2020).
- [20] A. B. Kuzmenko, *Rev. Sci. Instrum.* **76**, 083108 (2005).
- [21] L. Xie, J. H. Feng, R. Li, and J. Q. He, *Phys. Rev. Lett.* **125**, 245901 (2020).
- [22] B. Kh. Bairamov, Yu. E. Kitaev, V. K. Negoduiko, and Z. M. Khashkhozhev, *Fiz. Tverd. Tela* **16**, 2036 (1974) [*Sov. Phys. Solid State* **16**, 1323 (1975)].
- [23] S. Anand, P. Verma, K. Jain, and S. Abbi, *Phys. B: Condens. Matter* **226**, 331 (1996).